HHS Public Access

Author manuscript

ACS Appl Mater Interfaces. Author manuscript; available in PMC 2017 August 07.

Published in final edited form as:

ACS Appl Mater Interfaces. 2017 February 08; 9(5): 4425–4432. doi:10.1021/acsami.6b11536.

Virus-Inspired Self-Assembled Nanofibers with Aggregation-Induced Emission for Highly Efficient and Visible Gene Delivery

Chunqiu Zhang[†,‡], **Tingbin Zhang**[§,‡], **Shubin Jin**[†], **Xiangdong Xue**[†,ID], **Xiaolong Yang**[†], **Ningqiang Gong**[†], **Jinchao Zhang**[‖], **Paul C. Wang**[⊥,#], **Jian-Hua Tian**[§], **Jinfeng Xing**[§,*], and **Xing-Jie Liang**[†,*,ID]

[†]CAS Key Laboratory for Biological Effects of Nanomaterials & Nanosafety, National Center for Nanoscience and Technology, No. 11 Beiyitiao, Zhongguancun, Beijing 100190, China

[§]School of Chemical Engineering and Technology, Tianjin University, No. 92, Weijin Road, Nankai District, Tianjin 300072, China

[‖]College of Chemistry & Environmental Science, Chemical Biology Key Laboratory of Hebei Province, Hebei University, Baoding, 071002, China

[⊥]Laboratory of Molecular Imaging, Department of Radiology, Howard University, Washington, DC 20060, United States

[#]College of Science and Engineering, Fu Jen Catholic University, Taipei 24205, Taiwan

Abstract

High-efficiency gene transfer and suitably low cytotoxicity are the main goals of gene transfection systems based on nonviral vectors. In addition, it is desirable to track the gene transfer process in order to observe and explain the mechanism. Herein, inspired by viral structures that are optimized for gene delivery, we designed a small-molecule gene vector (TR4) with aggregation-induced emission properties by capping a peptide containing four arginine residues with tetraphenylethene (TPE) and a lipophilic tail. This novel vector can self-assemble with plasmid DNA to form nanofibers in solution with low cytotoxicity, high stability, and high transfection efficiency. pDNA@TR4 complexes were able to transfect a variety of different cell lines, including stem cells. The self-assembly process induces bright fluorescence from TPE, which makes the nanofibers visible by confocal laser scanning microscopy (CLSM). This allows us for the tracking of the gene delivery process.

[*]**Corresponding Authors**. jinfengxing@tju.edu.cn. liangxj@nanoctr.cn.

ORCID

Xiangdong Xue: 0000-0002-3709-072X

Xing-Jie Liang: 0000-0003-3806-6008

[‡]C.Z. and T.Z. contributed equally.

ASSOCIATED CONTENT

Supporting Information

The Supporting Information is available free of charge on the ACS Publications website at DOI: 10.1021/acsami.6b11536.

Materials and methods, HPLC trace and MALDI-TOFMS analysis of TR4, fluorescence spectra, cytotoxicity investigation, gene transfection, optical images, and cellular uptake inhibition results (PDF)

The authors declare no competing financial interest.

Graphical abstract

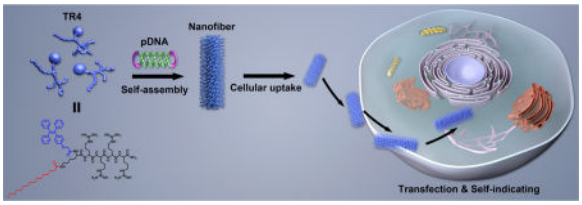

Keywords

gene delivery; peptide; nanofibers; transfection; self-indicating

INTRODUCTION

Efficient gene transfer into cells is widely used in biotechnological and medical areas, especially for gene silencing[1–3] and gene therapy.[4–6] In nature, viruses are the most efficient agent for gene transfer, and viruses have been widely used by scientists as vectors for gene delivery. However, viral vectors have the potential to introduce or generate infectious viruses, and this has driven the search for alternative nonviral gene delivery strategies. Many virus-like particles[7,8] and nanocarriers[9–13] have been developed for gene transfer. Although virus-like particles have been used successfully for gene expression and have a reduced risk of virus infection, the immunogenicity of the viral capsid protein must still be considered. The second approach to designing nonviral gene delivery systems (GDSs) is a supramolecular strategy, in which a positively charged region of the nanocarrier interacts with a gene and then takes the gene into cells. Sometimes, the gene is simply attached to the surface of the nanocarrier or entwined with hydrophilic polymers, but this usually does not sufficiently protect the gene from DNase degradation. Furthermore, the design of gene nanocarriers with high transfection efficiency and low cytotoxicity is still a challenge. Additionally, it is important to trace the gene transfer process, so that information on how the GDSs enter the cells and where they release the genes can be obtained. However, traditional GDSs are typically “one-trick ponies”, and their sole role is to deliver a gene into cells. It is hard to track the transfection process because of the lack of visible signals for observation. It is possible to add tags to the materials in the nanocarrier,[14,15] but this is complicated and can change the properties of the GDSs. Thus, the development of a novel GDS combining excellent stability, high transfection efficiency, and low cytotoxicity with self-indicating properties represents an important advance.

Motivated by this concept, we designed and synthesized a small-molecule gene vector (TR4) with aggregation-induced emission properties by capping a short peptide (four arginine residues) with a lipophilic tail and tetraphenylethene (TPE). The molecular structure of TR4 is shown in Figure 1. The design of this vector was mainly drafted from natural viruses and cell-penetrating peptides (CPPs). Natural viruses share common structural rules in that their capsid proteins interact with genes through a positively charged region and the whole structure is stabilized by noncovalent interactions between hydrophobic regions. We used similar rules to construct nonviral GDSs. For the positively charged region, we designed a

very short peptide composed of only four arginine residues, similar to the arginine-rich CPPs that have been identified as being highly efficient in cellular uptake and gene transfer.[16–20] It is known that arginine-rich CPPs are insufficient for highly effective transfection, even when they contain many arginine residues.[21,22] Adding more arginine residues to the sequence would increase the risk of cytotoxicity, so introducing noncovalent interactions from hydrophobic moieties would hopefully solve this problem and increase the transfection efficiency. Several studies have shown that capping CPPs with lipophilic tails[23] such as cholesteryl[24] and stearic acid[25] can dramatically increase their transfection efficiency. Thus, in this work, we modified the four arginine residues with two hydrophobic parts: palmitic acid (PA) and tetraphenylethene (TPE). More importantly, another purpose of introducing TPE was to make the vector visible by confocal laser scanning microscopy (CLSM). It is well-known that TPE, as a typical fluorescent dye with aggregation-induced emission (AIE) properties, shows high emission when it forms aggregates in water-based solutions,[26–30] unlike traditional organic dyes, which suffer from quenching in the aggregated state [aggregation-caused quenching (ACQ) effect].[31,32] When TPE-containing molecules self-assemble to form nanocarriers, the gene/vector complexes are visible under UV light because of the AIE properties of TPE. The presence of TPE will therefore confer imaging properties on the novel GDSs. We thus hypothesized that the conjugation of a lipophilic tail and TPE with very short arginine-rich CPPs should enhance the stability of the gene/vector complexes, just as for viruses. This should improve the transfection efficiency and allow for the tracking of the gene transfer process, which might result in a better-performing vector with multiple functions (Figure 1).

RESULTS AND DISCUSSION

Characterization of the Gene Binding Capacity of TR4

In this work, the novel vector with a unique molecular weight was directly obtained by standard solid-phase peptide synthesis (SPPS),[33] which is a very simple and low-cost method. The purity and molecular weight were confirmed by reverse-phase high-performance liquid chromatography (RPHPLC) and matrix-assisted laser desorption/ionization time-of-flight mass spectrometry (MALDI-TOF-MS) (Figure S1). To test the formation of the complex (denoted as pDNA@TR4) between plasmid DNA (pDNA) and TR4, agarose gel electrophoresis was used to determine the nitrogen-to-phosphorus ratio (N/P ratio) that is most efficient for fully condensing the pDNA. As shown in Figure 2A, pDNA was found to be retarded at a N/P ratio of 2 when we simply mixed pDNA and TR4 together in buffer solution. The electrophoresis results suggested that the pDNA was completely condensed by TR4 when the N/P ratio was 2 or greater. This was also confirmed by measuring the zeta potential of the pDNA@TR4 complexes formed at different N/P ratios. When the N/P ratio was greater than 2, the zeta potential was positive, demonstrating that the pDNA was completely assembled with TR4. The critical N/P ratio was calculated by isothermal titration calorimetry (ITC) (Figure 2B). As shown in Table 1, the critical ratio between nitrogen in TR4 and phosphorus in pDNA (N/P ratio) was found to be 1.69. This value is consistent with the agarose gel electrophoresis results, which showed that the pDNA was completely condensed by TR4 when the N/P ratio was increased to 2. The results also

indicated that ITC is a promising method for obtaining the critical N/P ratio for condensing DNA by nanovectors.

Determination of the Binding Stability of the pDNA@TR4 Complex

To compare the stability of this novel vector with those of traditional gene transfer vectors, poly-(ethylenimine) (PEI, M_n = 25000), a classical cationic polymer and an accepted standard for transfection,[34] was taken as a control. The binding affinities of TR4 and PEI with pDNA were evaluated by ITC titration (Table 1). The binding constants (K_a) for TR4 and PEI were found to be 2.38×10^7 M^{-1} and 2.19×10^5 M^{-1}, respectively. The K_a value of TR4 is 2 orders of magnitude higher than that of PEI, which demonstrates a stronger interaction between TR4 and pDNA. A competitive binding assay was also performed to test the binding affinities by separately mixing heparin (which has multiple negative charges) with the pDNA@TR4 and pDNA@PEI complexes. Figure 3A shows that, as the concentration of heparin was increased, pDNA bands appeared in the middle of the agarose gel in the PEI groups, indicating that the pDNA was dissociated from the pDNA@PEI complexes. This phenomenon was not observed for the TR4 groups. These results again indicate that the binding affinity between TR4 and pDNA is stronger, consistent with the ITC assay. The stabilities of the pDNA@TR4 and pDNA@PEI complexes were determined by DNase I treatment. Upon addition of DNase I, naked pDNA was completely degraded, and an increasing amount of the pDNA in pDNA@PEI complexes was degraded at longer incubation times, whereas the pDNA@TR4 complexes remained stable and intact (Figure 3B). We hypothesized that these distinct behaviors are based on the differences in the structures of TR4 and PEI. TR4 is an amphiphilic molecule and has a hydrophobic tail. When TR4 assembles with pDNA, its PA and TPE molecules can twist together to form a stable “capsid”, protecting the pDNA from dissociation and degradation.

Morphological and Luminescent Characterization of Nanofibers Formed by TR4 and pDNA

Traditional methods for transfection of long pDNAs have mainly focused on two strategies: One involves constructing the nanocarrier first and then attaching the plasmid to the surface of the carrier,[35–38] whereas the other uses a self-assembly approach to mix monodisperse polymers or small molecules with pDNA and then form gene/vector complexes in solution for transfection.[39–41] In this work, we found that, although TR4 has an amphiphilic structure, it exhibits good water solubility. By transmission electron microscopy (TEM), we found that TR4 could not form ordered aggregates in buffer solution when its concentration was less than 100 μM (Figure 4A). Also, because of the presence of the TPE molecules, which act as indicators of the aggregation state, fluorescence was observed under the UV lamp and fluorescence spectrophotometer when the TR4 molecules formed aggregates. As shown in Figure 4C, the free TR4 solution did not exhibit intrinsic fluorescence under a 365-nm UV lamp, as was also confirmed by the fluorescence spectrum (Figure S2). This indicates that TR4 was in a monodisperse state in solution. Once the pDNA was added to the TR4-containing solution and mixed, bright blue fluorescence could be observed under the UV lamp, indicating that self-assembly had occurred (Figure 4C). Fluorescence spectroscopy confirmed that the pDNA@TR4 complexes exhibited higher emission than free TR4 (Figure S2). Meanwhile, the optimal aggregation concentration and critical AIE concentration of TR4 with and without pDNA were investigated. We tested the fluorescence

intensity of TR4 and pDNA@TR4 complexes at TR4 concentrations of 10–100 μM. As shown in Figure S2A,B, the fluorescence intensity of the pDNA@TR4 complexes increased dramatically to several times that of TR4 without DNA. To further confirm the critical concentration, we calculated the ratio of the fluorescence intensity (at 466 nm) of the pDNA@TR4 complexes (I_C) to the fluorescence intensity of TR4 (I_0). As shown in Figure S2C, as the concentration of TR4 was increased to 60 μM, the I_C/I_0 ratio also increased. In addition, the I_C/I_0 ratio reached its maximum value when the concentration of TR4 was in the range of 60–80 μM. Then, the I_C/I_0 ratio began to drop because of the aggregation of TR4 itself when the concentration was increased further. Thus, the optimal concentration of TR4 in the work was found to be 60–80 μM. To our surprise, TEM imaging of the pDNA@TR4 complexes demonstrated a kind of nanofiber structure, with the fibers having lengths in the range of micrometers and widths of approximately 50–100 nm (Figure 4B). To further confirm that TR4 and pDNA were both present in the assembled structures, we labeled the pDNA with Cy5, an organic dye that emits red fluorescence, to observe the colocalization with TR4 by confocal laser scanning microscopy (CLSM). As shown in Figure 4D–F, the blue color (TPE) of TR4 and the red color (Cy5) of pDNA were merged together, indicating coassembly. Although the exact internal structure of these nanofibers remains unclear, it is interesting to have constructed such a gene delivery system by self-assembly of a CPP analogue in the presence of pDNA.

pDNA@TR4-Mediated Gene Delivery and Expression in Different Cell Lines

As described above, zeta potential measurements showed that the surface of the nanofibers was positively charged when the N/P ratio was greater than 2. Therefore, the cytotoxicity and transfection efficiency of pDNA@TR4 nanofibers at N/P ratios of 3 and 4 were tested after the complexes had been incubated with cells for 24 and 48 h, respectively. As a control, the same measurements were performed for pDNA@PEI at a N/P ratio of 10. From an MTT assay, we found that, even when the N/P ratio was increased to 4, there was no particularly obvious cytotoxicity in several types of cell line for pDNA@TR4 nanofibers, indicating that this novel vector has good biocompatibility (Figure S3). We then optimized the amount of pDNA for gene transfection in HeLa cells and found that 2 μg of pDNA in pDNA@TR4 nanofibers was the best dose (Figure S4). To investigate the universal applicability of this novel vector for gene transfection in different cell lines, we incubated pDNA@TR4 and pDNA@PEI with cancer cells (HeLa and HepG2 cells), normal cells (NIH 3T3 and 293T cells), and even stem cells (R1 cells), using pDNA expressing an enhanced green fluorescent protein (EGFP). As shown in Figure 5, the transfection efficiency of pDNA@TR4 in HeLa cells was nearly 70% at a N/P ratio of 4 and 55% at a lower N/P ratio of 3, whereas the transfection efficiency of pDNA@PEI was just 15% in HeLa cells. In another cancer cell line, HepG2, pDNA@PEI showed even lower transfection efficiency (no more than 5%), but the pDNA@TR4 nanofibers still achieved 50% transfection efficiency (Figures 5 and S5). In NIH 3T3 cells, almost no EGFP was expressed using pDNA@PEI, compared to a high transfection efficiency of 40–50% observed in the pDNA@TR4 groups (Figure 5). The only cell line in which pDNA@PEI presented a higher transfection efficiency than pDNA@TR4 was 293T cells (Figures 5 and S6). The transfection efficiency of the commercial transfection reagent Lipofectamine 2000 was also tested as a control. As shown in Figures S7 and S8, the pDNA@TR4 nanofibers showed a much higher transfection efficiency than

PEI and Lipofectamine 2000 in HepG2 cells. More importantly, in this work, the novel GDS achieved a transfection efficiency of approximately 15% in stem cells (Figure 5). Thus, TR4 is a potential novel vector for gene delivery in stem cells.

Characterization of the Self-Indicating Property and Uptake Pathway of pDNA@TR4 Nanofibers in Cells

The self-indicating property of this novel vector was investigated using CLSM. As in the experimental results shown in Figure 4, the pDNA was labeled with Cy5 so that there were three colors to identify and trace the pDNA (Cy5, red color), TR4 (TPE, blue color), and pDNA@TR4 (merged, purple color). Concurrently, the lysosomes in HeLa cells were stained with LysoTracker Green. As shown in Figure 6, within the first 4 h, the pDNA and TR4 remained coassembled, and the pDNA@TR4 nanofibers were mainly attached to the surface of cell membranes. To further confirm that the nanofibers were located on the surface of the cell membranes, we labeled the cell membranes with DiI, a commercial cell membrane tracker, and checked its colocalization with pDNA@TR4 nanofibers for 4 h, as shown in Figure S9. In Figure S9D,F, the results show that the pDNA@TR4 nanofibers (purple color) merged very well with the cell membrane tracker DiI (green color). This means that the pDNA@TR4 nanofibers mainly attached to the surface of the cell membranes within the first 4 h. After 24 h of incubation, the nanofibers entered into the cells, and some red-colored points appeared but did not merge with lysosomes, indicating that a portion of the pDNA was released from the nanofibers and escaped from the lysosomes. To further investigate the cellular uptake pathway, a series of inhibitors were employed (Figure S10). Chlorpromazine hydrochloride and genistein are inhibitors of clathrin- and caveolae-mediated endocytosis, respectively, whereas dynasore, a dynamin-GTPase inhibitor, can inhibit the two types of internalization simultaneously. 5-*N*-ethyl-*N*-isopropyl amiloride (EIPA) and amiloride hydrochloride are inhibitors of macropinocytosis/phagocytosis. Also, low temperature (4 °C) was used to decrease the energy-dependent internalization. We found that the uptake of pDNA@TR4 nanofibers occurred by the energy-dependent and clathrin- and caveolae-dependent internalization pathways.

CONCLUSIONS

In this work, we have successfully developed a novel nanofiber gene delivery system by using a CPP-analogue-assisted pDNA self-assembly strategy. Compared to traditional vectors such as PEI, this system showed good stability and biocompatibility and exhibited much higher transfection efficacies in many kinds of cell lines, even in stem cells. Furthermore, it also displayed self-indicating properties for tracing the gene delivery process in vitro. On the basis of these concepts, we plan to design and develop other efficient and visible gene delivery systems with superior performance for biotechnological and medical applications in the near future.

EXPERIMENTAL SECTION

Preparation of pDNA@TR4 Nanofibers

First, TR4 powder was dissolved in pure water to make a 1 mM TR4 stock solution. Then, 72 μL of the TR4 stock solution was mixed with 24.0 μg of EGFP-N1 plasmid DNA and stored at room temperature for 30 min to form the complex.

Mouse Stem Cell (R1) Culture

Mouse embryonic feeder (MEF) cells were prepared as follows: The uterus was removed from a pregnant mouse with scissors and put into a plate containing phosphate-buffered saline (PBS). The amnion was removed by forceps to release the embryos, which were transferred to a new PBS plate. The embryos were then dissected, and the trunk was put into a new PBS plate after the head, tail, limbs, and liver had been removed. The trunk was cut into pieces in a small amount of PBS; then 0.05% trypsin was added, and the plate was inverted repeatedly for 2 min before the solution was neutralized with 10% fetal bovine serum (FBS) medium. Next, the cell-containing supernatant was transferred into a new 50 mL tube, and the trypsinization/neutralization step was repeated three times until the cell clumps disappeared. The tube was centrifuged, and the pelleted cells (MEF cells) were suspended in new medium for plating onto dishes. The feeder cells were cultured for 12 h until they had grown to an appropriate density. Finally, mouse R1 stem cells were plated on the MEF cells.

Transfection

The solution of pDNA@TR4 complexes was diluted into 1.2 mL of 5% dextrose solution to make a pDNA@TR4 stock solution for transfection. The stock solution became visibly fluorescent upon mixing of TR4 with pDNA, indicating successful construction of the pDNA@TR4 complexes. The cells were seeded at 8×10^4 cells per well in 12-well plates and cultured in 1 mL of Dulbecco's Modified Eagle Medium with high glucose (H-DMEM) supplemented with 10% FBS, 100 mg/mL streptomycin and 100 U/mL penicillin for 24 h. Before transfection, the culture medium was replaced by Opti-MEM (reduced-serum medium) for 15 min to starve the cells. Then, the Opti-MEM medium was replaced by pDNA@TR4 complexes diluted in 1 mL of Opti-MEM (2 μg of pDNA in each well). Four hours later, the complex-containing medium was exchanged with supplemented H-DMEM, and culturing was continued for another 44 h. The images of EGFP expression of each sample were taken by inverted fluorescence microscopy, and the level of transfection efficiency was determined by flow cytometry.

Cytotoxicity Studies

Cells were planted at a density of 5×10^3 cells/well in 96-well plate and precultured for 24 h. Subsequently, the cells were treated with pDNA@TR4 (containing 0.2 μg of pDNA) with N/P ratios varying from 1/1 to 4/1 and pDNA@PEI at a N/P ratio of 10 (containing 0.2 μg of pDNA) for another 24 h. To quantify the cell viability of each sample, the medium was exchanged with 100 μL of 0.5 mg/mL 3-(4,5-dimethylthiazol-2-yl)-2,5-diphenyltetrazolium bromide (MTT) diluted with basic medium and cultured for 2 h. Then, the MTT solution

was aspirated and replaced with 150 μL of dimethyl sulfoxide (DMSO) solution. The absorbance of each well at 570 nm was quantified using an Infinite M200 microplate reader (TECAN, San Jose, CA). All of the experiments were carried out with five replicates.

Subcellular Localization and Imaging

HeLa cells were seeded into a 35-mm glass dish at a density of 8×10^4 cells and incubated for 24 h at 37 °C; subsequently, they were treated with pDNA@TR4 (containing 2 μg of pDNA modified by Cy5) at a N/P ratio of 4 for 4 and 24 h. The cells were then stained with LysoTracker Green for 14 min, after which they were washed three times with PBS and imaged by CLSM with excitation at 405 nm for TPE, 488 nm for LysoTracker Green, and 633 nm for Cy5.

Analysis of the Cellular Uptake Pathway for pDNA@TR4 in HeLa Cells

HeLa cells were seeded in a 24-well plate at a density of 5×10^4 cells per well 24 h in advance. The cells were precultured with different concentrations of inhibitors diluted with basic medium for 30 min. For treatment at low temperature, cells were incubated at 4 °C in a refrigerator. The transfection process of this part was the same as that described in the Transfection section. pDNA@TR4 at a N/P ratio of 4 was used. Cells treated with pDNA@TR4 (containing 1 μg of pDNA) and no inhibitor treatment served as the control, and their expression efficiency was set as 100%. The inhibitor concentrations were applied as follows: chlorpromazine hydrochloride (Ch), 15–45 μM; genistein (Ge), 100–300 μM; dynasore (Dy), 40–120 μM; 5-*N*ethyl-*N*-isopropyl amiloride (EIPA), 5–15 μM; and amiloride hydrochloride (Am), 50–150 μM.

Acknowledgments

This work was financially supported in part by grants from the Chinese Natural Science Foundation Key Project (Grant 31430031), the National Natural Science Foundation of China (Grant 31371014), and the State High-Tech Development Plan (Grants 2012AA020804 and SS2014AA020708), as well as a National Distinguished Young Scholars grant (Grant 31225009). The authors also appreciate the support from the Strategic Priority Research Program of the Chinese Academy of Sciences (Grant XDA09030301); the external cooperation program of BIC, Chinese Academy of Sciences (Grant 121D11KYSB20130006); and the U.S. NIH/NIMHD (Grant G12MD007597)

References

1. Kam NW, Liu Z, Dai H. Functionalization of Carbon Nanotubes via Cleavable Disulfide Bonds for Efficient Intracellular Delivery of siRNA and Potent Gene Silencing. J. Am. Chem. Soc. 2005; 127:12492–12493. [PubMed: 16144388]
2. Minakuchi Y, Takeshita F, Kosaka N, Sasaki H, Yamamoto Y, Kouno M, Honma K, Nagahara S, Hanai K, Sano A, Kato T, Terada M, Ochiya T. Atelocollagen-Mediated Synthetic Small Interfering RNA Delivery for Effective Gene Silencing in Vitro and in Vivo. Nucleic. Acids. Res. 2004; 32:e109. [PubMed: 15272050]
3. Rubinson DA, Dillon CP, Kwiatkowski AV, Sievers C, Yang L, Kopinja J, Rooney DL, Zhang M, Ihrig MM, McManus MT, Gertler FB, Scott ML, Van Parijs L. A Lentivirus-Based System to Functionally Silence Genes in Primary Mammalian Cells, Stem Cells and Transgenic Mice by RNA Interference. Nat. Genet. 2003; 33:401–406. [PubMed: 12590264]
4. El-Aneed A. An Overview of Current Delivery Dystems in Cancer Gene Therapy. J. Controlled Release. 2004; 94:1–14.
5. Niidome T, Huang L. Gene Therapy Progress and Prospects: Nonviral Vectors. Gene Ther. 2002; 9:1647–1652. [PubMed: 12457277]

6. Herweijer H, Wolff JA. Gene Therapy Progress and Prospects: Hydrodynamic Gene Delivery. Gene Ther. 2007; 14:99–107. [PubMed: 17167496]
7. Kay MA, Glorioso JC, Naldini L. Viral Vectors for Gene Therapy: the Art of Turning Infectious Aagents into Vvehicles of Therapeutics. Nat. Med. 2001; 7:33–40. [PubMed: 11135613]
8. Krauzewicz N, Stokrova J, Jenkins C, Elliott M, Higgins CF, Griffin BE. Virus-Like Gene Transfer into Cells Mediated by Polyoma Virus Pseudocapsids. Gene Ther. 2000; 7:2122–2131. [PubMed: 11223994]
9. Pack DW, Hoffman AS, Pun S, Stayton PS. Design and Development of Polymers for Gene Delivery. Nat. Rev. Drug Discovery. 2005; 4:581–593. [PubMed: 16052241]
10. Patil ML, Zhang M, Minko T. Multifunctional Triblock Nanocarrier (PAMAM-PEG-PLL) for the Efficient Intracellular siRNA Delivery and Gene Silencing. ACS Nano. 2011; 5:1877–1887. [PubMed: 21322531]
11. Tian H, Chen J, Chen X. Nanoparticles for Gene Delivery. Small. 2013; 9:2034–2044. [PubMed: 23630123]
12. Guo X, Huang L. Recent Advances in Nonviral Vectors for Gene Delivery. Acc. Chem. Res. 2012; 45:971–979. [PubMed: 21870813]
13. Ganta S, Devalapally H, Shahiwala A, Amiji M. A Review of Stimuli-Responsive Nanocarriers for Drug and Gene Delivery. J. Controlled Release. 2008; 126:187–204.
14. Godbey WT, Wu KK, Mikos AG. Tracking the Intracellular Path of Poly(ethylenimine)/DNA Complexes for Gene Delivery. Proc. Natl. Acad. Sci. U. S. A. 1999; 96:5177–5181. [PubMed: 10220439]
15. Shi B, Zhang H, Qiao SZ, Bi J, Dai S. Intracellular Microenvironment-Responsive Label-Free Autofluorescent Nanogels for Traceable Gene Delivery. Adv. Healthcare Mater. 2014; 3:1839–1848.
16. Crombez L, Aldrian-Herrada G, Konate K, Nguyen QN, McMaster GK, Brasseur R, Heitz F, Divita G. A New Potent Secondary Amphipathic Cell-Penetrating Peptide for siRNA Delivery into Mammalian Cells. Mol. Ther. 2009; 17:95–103. [PubMed: 18957965]
17. Zorko M, Langel U. Cell-Penetrating Peptides: Mechanism and Kinetics of Cargo Delivery. Adv. Drug Delivery Rev. 2005; 57:529–545.
18. Milletti F. Cell-Penetrating Peptides: Classes, Origin, and Current Landscape. Drug Discovery Today. 2012; 17:850–860. [PubMed: 22465171]
19. Li M, Schlesiger S, Knauer SK, Schmuck C. A Tailor-Made Specific Anion-Binding Motif in the Side Chain Transforms a Tetrapeptide into an Efficient Vector for Gene Delivery. Angew. Chem., Int. Ed. 2015; 54:2941–2944.
20. Douat C, Aisenbrey C, Antunes S, Decossas M, Lambert O, Bechinger B, Kichler A, Guichard G. A Cell-Penetrating Foldamer with a Bioreducible Linkage for Intracellular Delivery of DNA. Angew. Chem., Int. Ed. 2015; 54:11133–11137.
21. Futaki S, Suzuki T, Ohashi W, Yagami T, Tanaka S, Ueda K, Sugiura Y. Arginine-rich peptides. An Abundant Source of Membrane-Permeable Peptides Having Potential as Carriers for Intracellular Protein Delivery. J. Biol. Chem. 2001; 276:5836–5840. [PubMed: 11084031]
22. Tunnemann G, Ter-Avetisyan G, Martin RM, Stockl M, Herrmann A, Cardoso MC. Live-Cell Analysis of Cell Penetration Ability and Toxicity of Oligo-Arginines. J. Pept. Sci. 2008; 14:469–476. [PubMed: 18069724]
23. Kuchelmeister HY, Karczewski S, Gutschmidt A, Knauer S, Schmuck C. Utilizing Combinatorial Chemistry and Rational Design: Peptidic Tweezers with Nanomolar Affinity to DNA Can Be Transformed into Efficient Vectors for Gene delivery by Addition of a Lipophilic Tail. Angew. Chem., Int. Ed. 2013; 52:14016–14020.
24. Kim WJ, Christensen LV, Jo S, Yockman JW, Jeong JH, Kim YH, Kim SW. Cholesteryl Oligoarginine Delivering Vascular Endothelial Growth Factor siRNA Effectively Inhibits Tumor Growth in Colon Adenocarcinoma. Mol. Ther. 2006; 14:343–350. [PubMed: 16765648]
25. Futaki S, Ohashi W, Suzuki T, Niwa M, Tanaka S, Ueda K, Harashima H, Sugiura Y. Stearylated Arginine-Rich Peptides: A New Class of Transfection Systems. Bioconjugate Chem. 2001; 12:1005–1011.

26. Zhang C, Jin S, Li S, Xue X, Liu J, Huang Y, Jiang Y, Chen WQ, Zou G, Liang XJ. Imaging Intracellular Anticancer Drug Delivery by Self-Assembly Micelles with Aggregation-Induced Emission (AIE Micelles). ACS Appl. Mater. Interfaces. 2014; 6:5212–5220. [PubMed: 24606837]
27. Zhang C, Liu C, Xue X, Zhang X, Huo S, Jiang Y, Chen WQ, Zou G, Liang XJ. Salt-Responsive Self-Assembly of Luminescent Hydrogel with Intrinsic Gelation-Enhanced Emission. ACS Appl. Mater. Interfaces. 2014; 6:757–762. [PubMed: 24372361]
28. Liang J, Tang BZ, Liu B. Specific Light-up Bioprobes Based on AIEgen Conjugates. Chem. Soc. Rev. 2015; 44:2798–2811. [PubMed: 25686761]
29. Kwok RT, Leung CW, Lam JW, Tang BZ. Biosensing by Luminogens with Aggregation-Induced Emission Characteristics. Chem. Soc. Rev. 2015; 44:4228–4238. [PubMed: 25374162]
30. Hong Y, Lam JW, Tang BZ. Aggregation-Induced Emission. Chem. Soc. Rev. 2011; 40:5361–5388. [PubMed: 21799992]
31. Jenekhe SA, Osaheni JA. Excimers and Exciplexes of Conjugated Polymers. Science. 1994; 265:765–768. [PubMed: 17736274]
32. Grabowski ZR, Rotkiewicz K, Rettig W. Structural Changes Accompanying Intramolecular Electron Transfer: Focus on Twisted Intramolecular Charge-Transfer States and Structures. Chem. Rev. 2003; 103:3899–4032. [PubMed: 14531716]
33. Zhang C, Jin S, Yang K, Xue X, Li Z, Jiang Y, Chen WQ, Dai L, Zou G, Liang XJ. Cell Membrane Tracker Based on Restriction of Intramolecular Rotation. ACS Appl. Mater. Interfaces. 2014; 6:8971–8975. [PubMed: 24878872]
34. Godbey WT, Wu KK, Mikos AG. Poly(ethylenimine) and Its Role in Gene Delivery. J. Controlled Release. 1999; 60:149–160.
35. Han L, Zhao J, Zhang X, Cao W, Hu X, Zou G, Duan X, Liang XJ. Enhanced siRNA Delivery and Silencing Gold-Chitosan Nanosystem with Surface Charge-Reversal Polymer Assembly and Good Biocompatibility. ACS Nano. 2012; 6:7340–7351. [PubMed: 22838646]
36. Guo S, Huang Y, Jiang Q, Sun Y, Deng L, Liang Z, Du Q, Xing J, Zhao Y, Wang PC, Dong A, Liang XJ. Enhanced Gene Delivery and siRNA Silencing by Gold Nanoparticles Coated with Charge-Reversal Polyelectrolyte. ACS Nano. 2010; 4:5505–5511. [PubMed: 20707386]
37. Karimi M, Ghasemi A, Sahandi Zangabad P, Rahighi R, Moosavi Basri SM, Mirshekari H, Amiri M, Shafaei Pishabad Z, Aslani A, Bozorgomid M, Ghosh D, Beyzavi A, Vaseghi A, Aref AR, Haghani L, Bahrami S, Hamblin MR. Smart Micro/Nanoparticles in Stimulus-Responsive Drug/Gene Delivery Systems. Chem. Soc. Rev. 2016; 45:1457–1501. [PubMed: 26776487]
38. Loh XJ, Lee TC, Dou Q, Deen GR. Utilising Inorganic Nanocarriers for Gene Delivery. Biomater. Sci. 2016; 4:70–86. [PubMed: 26484365]
39. Ni R, Chau Y. Structural Mimics of Viruses through Peptide/DNA Co-Assembly. J. Am. Chem. Soc. 2014; 136:17902–17905. [PubMed: 25389763]
40. Xu P, Li SY, Li Q, Van Kirk EA, Ren J, Murdoch WJ, Zhang Z, Radosz M, Shen Y. Virion-Mimicking Nanocapsules from pH-Controlled Hierarchical Self-Assembly for Gene Delivery. Angew. Chem., Int. Ed. 2008; 47:1260–1264.
41. Li M, Ehlers M, Schlesiger S, Zellermann E, Knauer SK, Schmuck C. Incorporation of A Non-Natural Arginine Analogue into a Cyclic Peptide Leads to Formation of Positively Charged Nanofibers Capable of Gene Transfection. Angew. Chem., Int. Ed. 2016; 55:598–601.

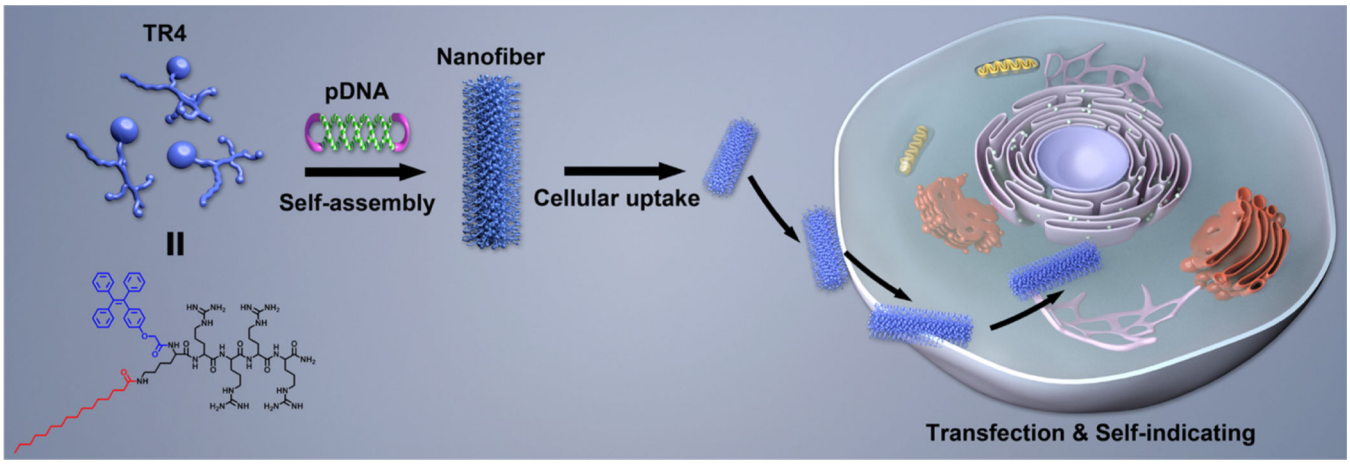

Figure 1.
Schematic illustration of the formation and transfection of AIE nanofibers constructed from TR4 and plasmid DNA for traceable gene delivery.

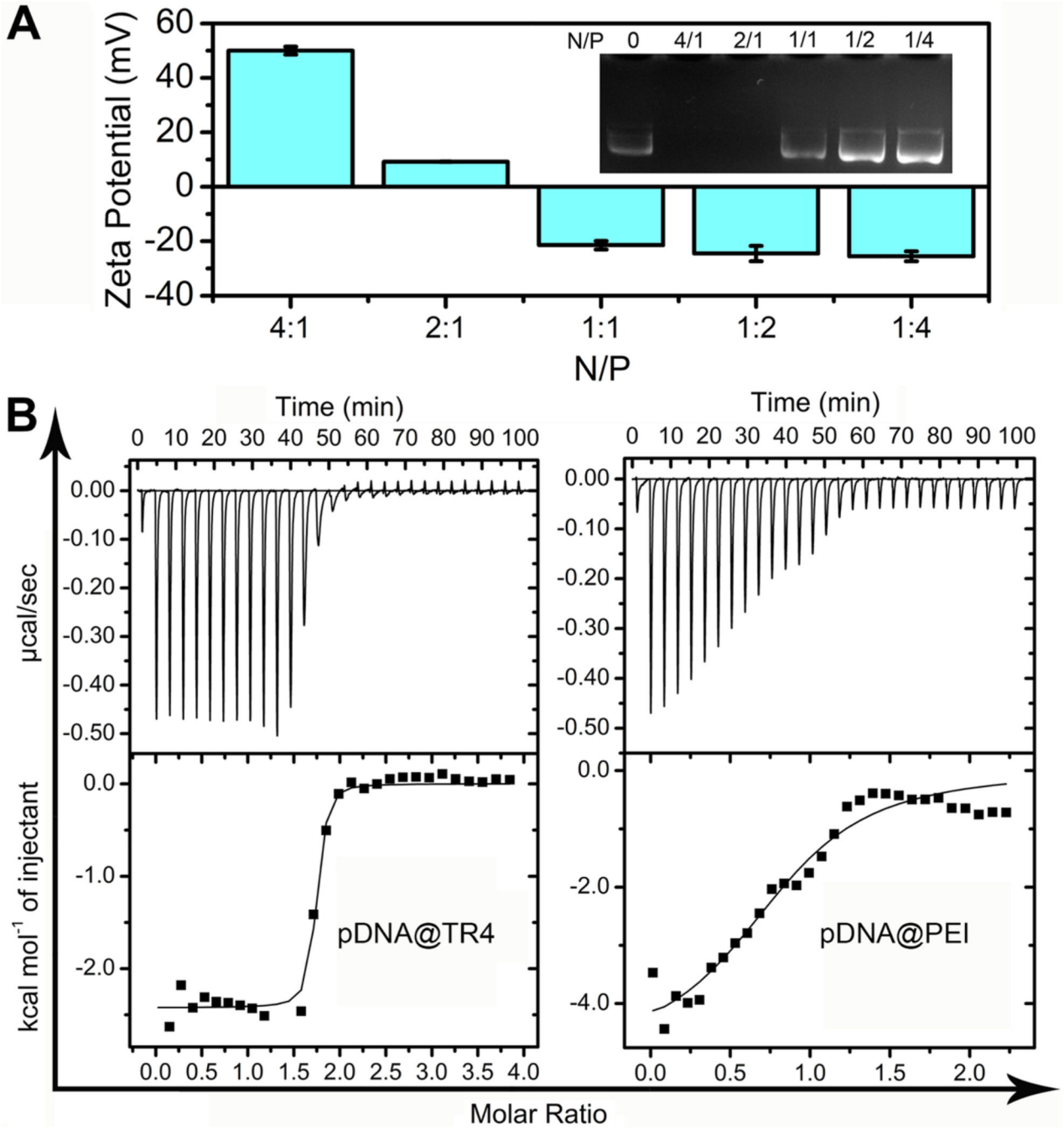

Figure 2.

(A) Zeta potential of pDNA@TR4 complexes and image showing the migration of the complexes in an agarose gel. The N/P ratios of the pDNA@TR4 complexes varied from 4/1 to 1/4 (N/P = 0 corresponds to free pDNA). (B) Isothermal titration calorimetry (ITC) titration in deionized water: TR4 (N in TR4 is 0.54 mM) or PEI (N in PEI is 0.31 mM) was added to pDNA (P in pDNA is 0.03 mM).

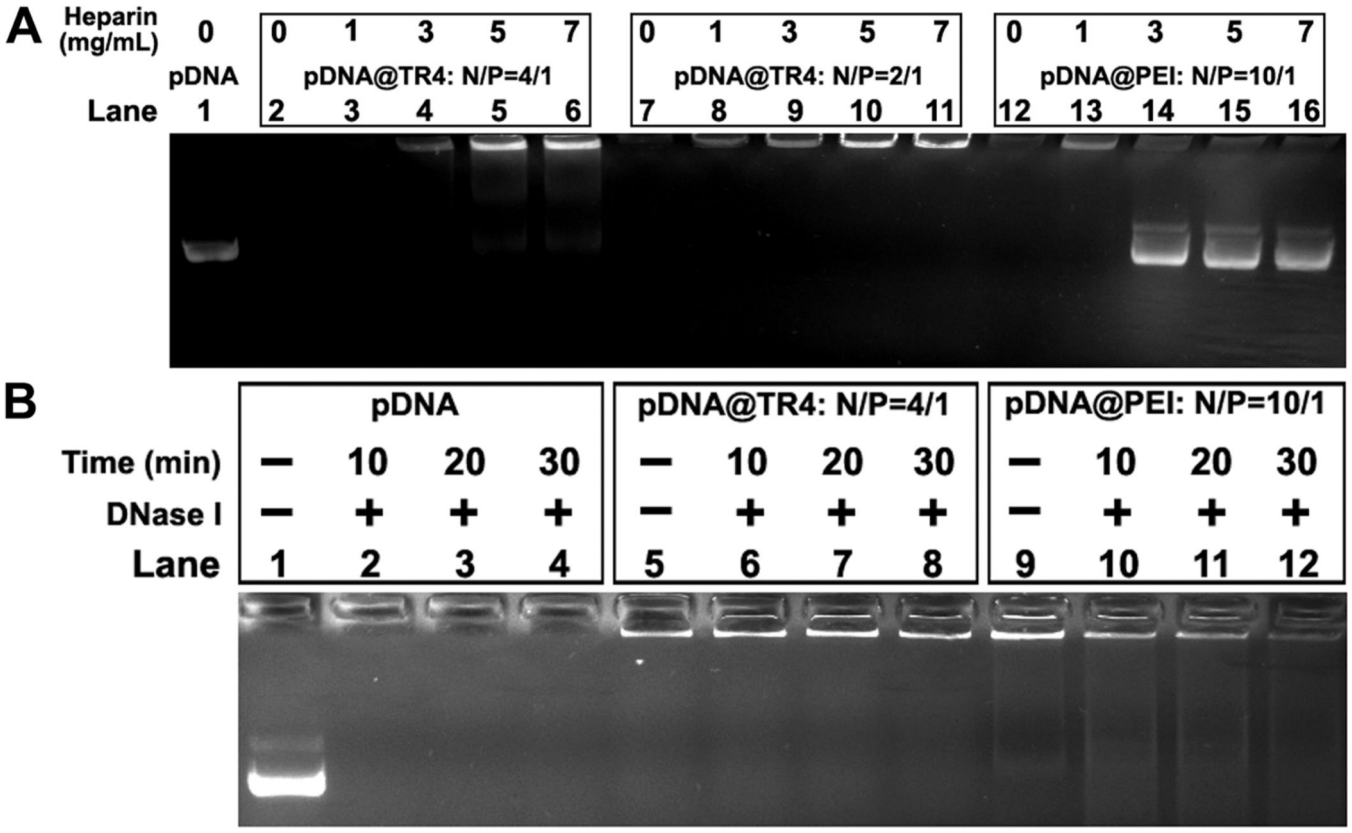

Figure 3.

(A) Heparin competitive binding assay. Lanes 1, 7, 12: pDNA control, pDNA@TR4, and pDNA@PEI without heparin treatment, respectively. Lanes 3–6: pDNA@TR4 at a N/P ratio of 4 treated with heparin at concentrations of 1, 3, 5, and 7 mg/mL, respectively. Lanes 8–11: pDNA@TR4 at a N/P ratio of 2 treated with heparin at concentrations of 1, 3, 5, and 7 mg/mL, respectively. Lanes 13–16: pDNA@PEI treated with heparin at concentrations of 1, 3, 5, and 7 mg/mL, respectively. (B) DNase I digestion assay. Lanes 1, 5, 9: pDNA control, pDNA@TR4, and pDNA@PEI without DNase I treatment, respectively. Lanes 2–4: Naked pDNA treated with DNase I for 10, 20, and 30 min, respectively. Lanes 6– 8: pDNA@TR4 treated with DNase I for 10, 20, and 30 min, respectively. Lanes 10–12: pDNA@PEI treated with DNase I for 10, 20, and 30 min, respectively.

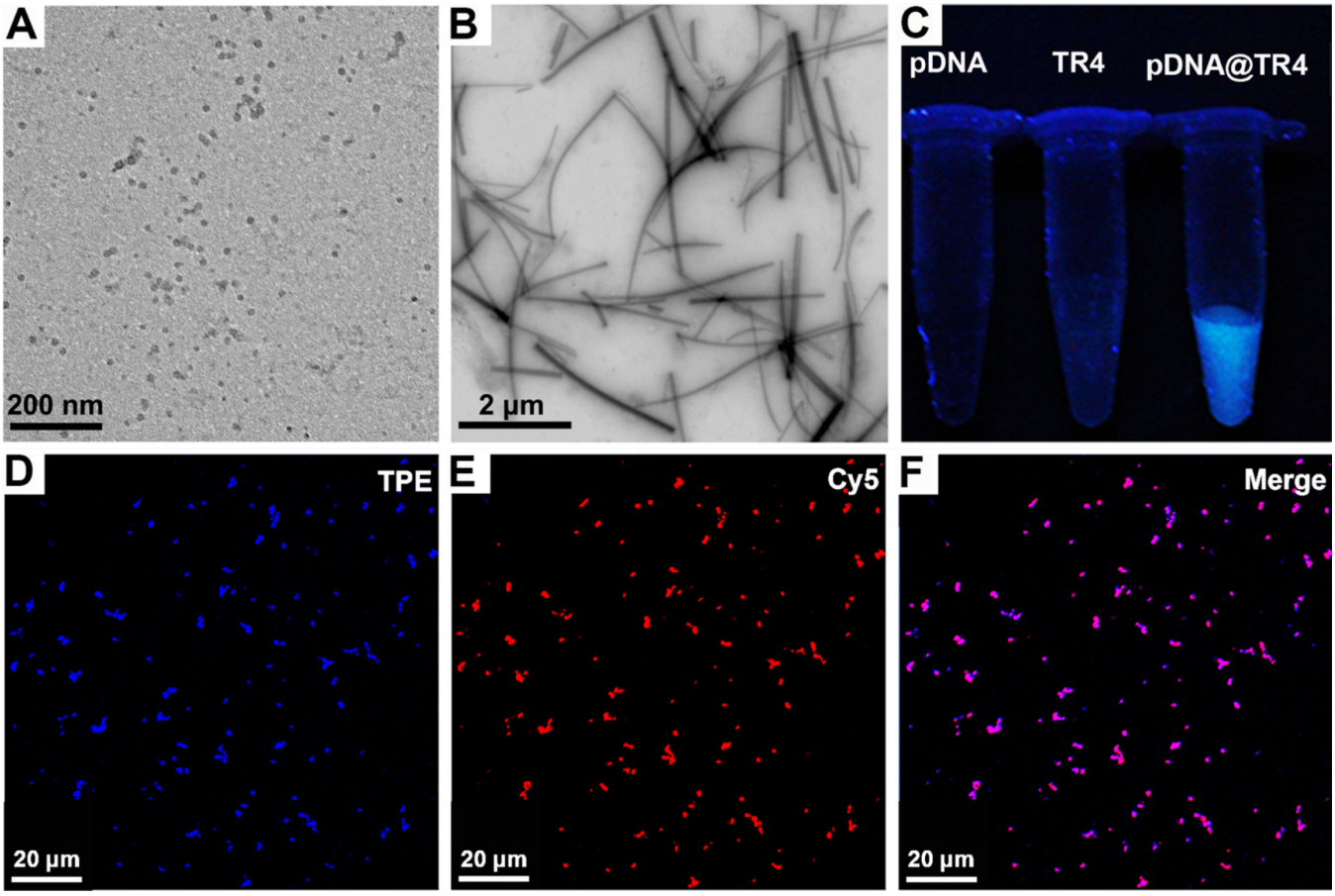

Figure 4.

(A,B) TEM images of (A) free TR4 (70 μM) and (B) pDNA@TR4 complexes at a N/P ratio of 4 (the concentration of TR4 was 70 μM). (C) Fluorescence images under a 365-nm UV lamp of pDNA, free TR4 (25 μM), and pDNA@TR4 complexes at a N/P ratio of 4 (the concentration of TR4 was 25 μM. (D–F) CLSM images of pDNA@TR4 complexes at a N/P ratio of 4 (the concentration of TR4 was 70 μM): (D) TR4 image, (E) Cy5-labeled pDNA image, and merged image of panels D and E.

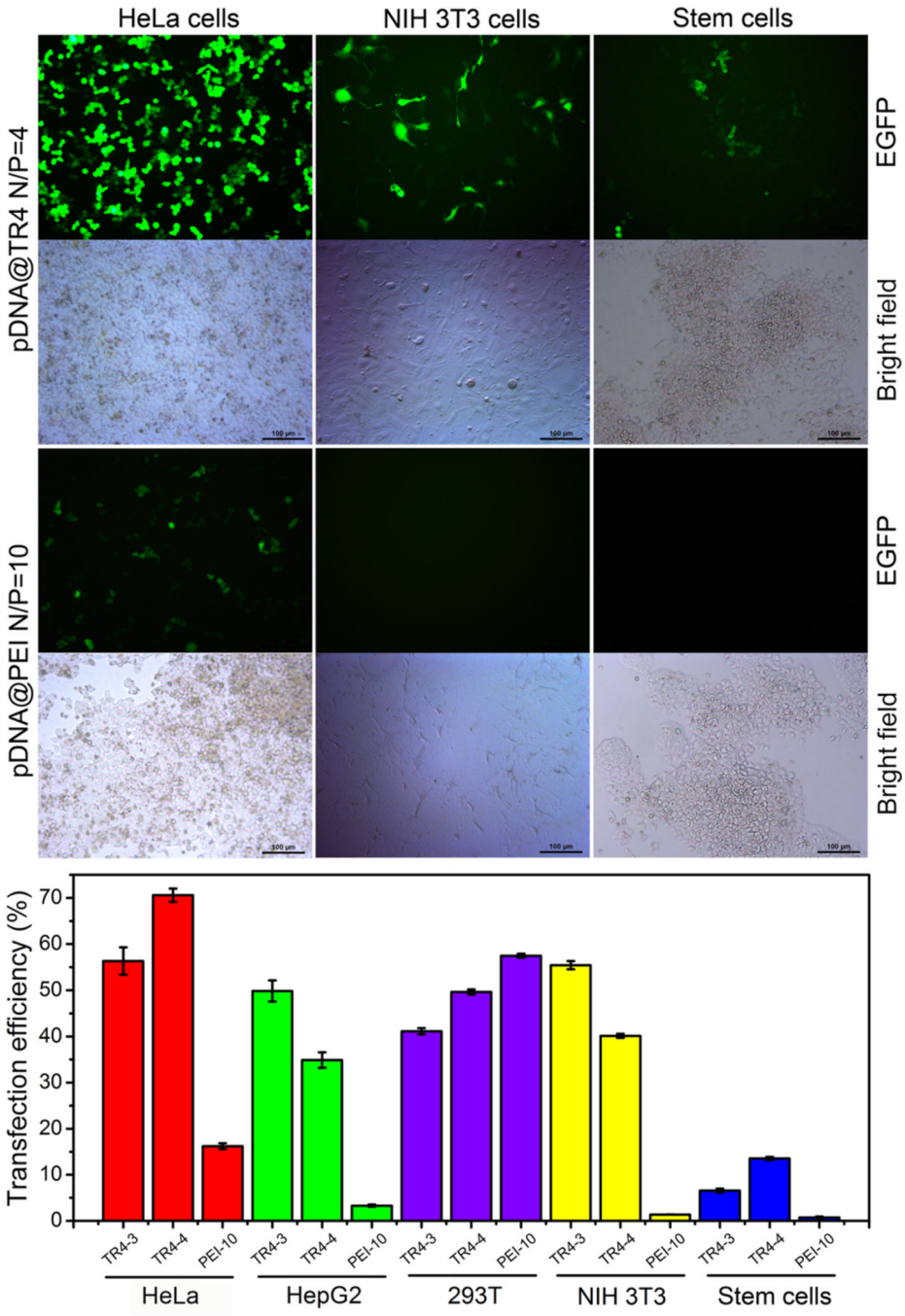

Figure 5.

Transfection of different cell lines with 2 μg of EGFP-N1 plasmid using pDNA@TR4 or pDNA@PEI complexes. (Top) Fluorescence images and (bottom) transfection efficiencies of different cell lines 48 h after transfection with pDNA@TR4 or pDNA@PEI (TR4-3 means that the N/P ratio was 3/1, TR4-4 means that the N/P ratio was 4/1, and PEI-10 means that the N/P ratio was 10/1).

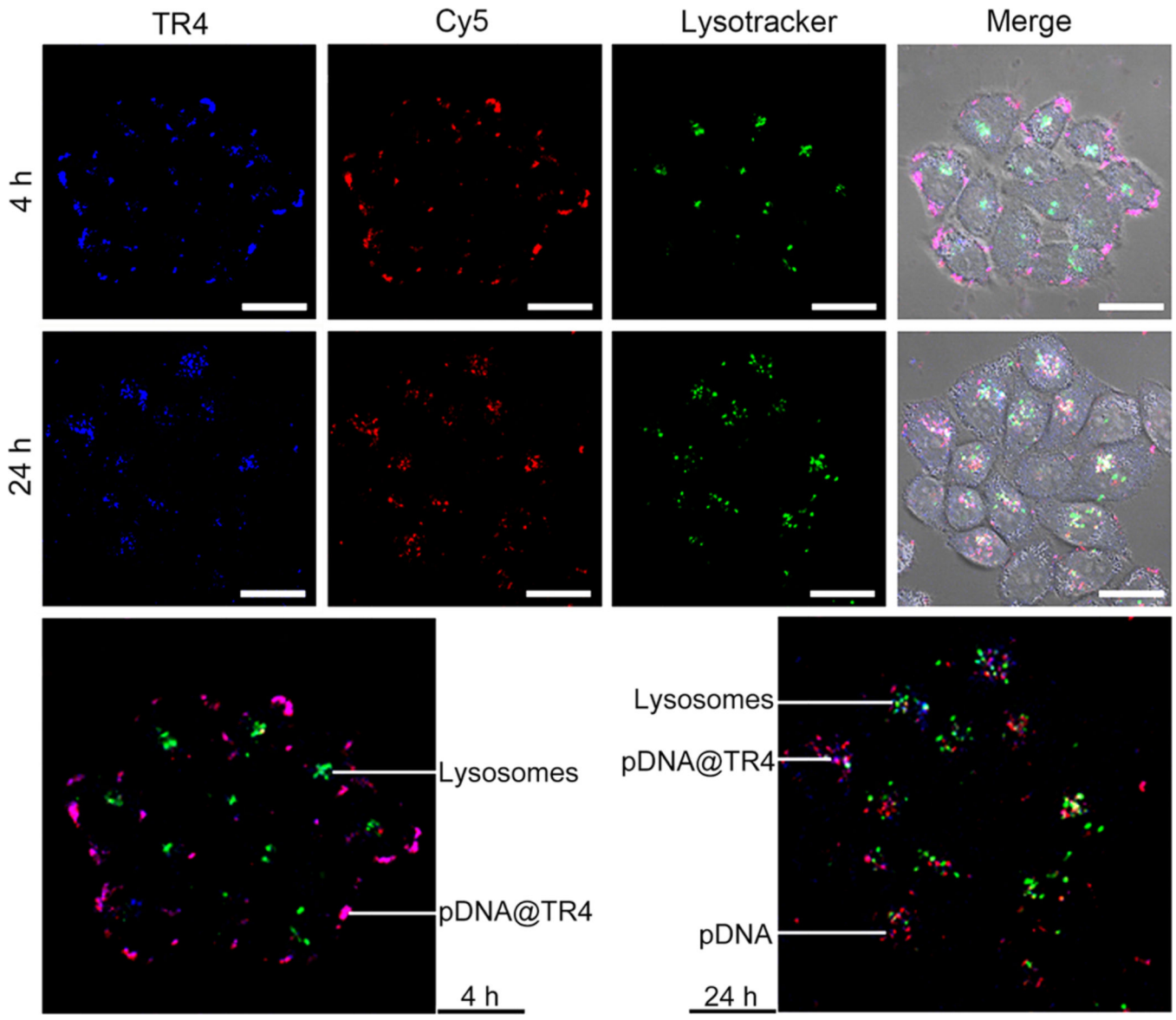

Figure 6.

CLSM images of cells treated with pDNA@TR4 nanofibers. TR4 was labeled with TPE (blue). The pDNA was labeled with Cy5 (red), and lysosomes were detected with LysoTracker Green. HeLa cells were incubated with pDNA@TR4 nanofibers for 4 and 24 h. Scale bars are 20 μm.

Table 1

Results of Isothermal Titration Calorimetry (ITC) Titrations

sample	K_a (M^{-1})	ΔH (cal/mol)	ΔS (cal/mol/deg)	N (sites)
pDNA@TR4	2.38×10^7	−2424.00	25.60	1.69
pDNA@PEI	2.19×10^5	−4885.00	8.05	0.84